

## PdGa intermetallic hydrogenation catalyst: an NMR and physical property study

This article has been downloaded from IOPscience. Please scroll down to see the full text article.

2012 J. Phys.: Condens. Matter 24 085703

(<http://iopscience.iop.org/0953-8984/24/8/085703>)

View [the table of contents for this issue](#), or go to the [journal homepage](#) for more

Download details:

IP Address: 193.2.6.70

The article was downloaded on 08/02/2012 at 07:56

Please note that [terms and conditions apply](#).

# PdGa intermetallic hydrogenation catalyst: an NMR and physical property study

M Klanjšek<sup>1,2</sup>, A Gradišek<sup>1</sup>, A Kocjan<sup>1,3</sup>, M Bobnar<sup>1</sup>, P Jeglič<sup>1,2</sup>,  
M Wencka<sup>4</sup>, Z Jagličič<sup>5</sup>, P Popčević<sup>6</sup>, J Ivkov<sup>6</sup>, A Smontara<sup>6</sup>, P Gille<sup>7</sup>,  
M Armbrüster<sup>8</sup>, Yu Grin<sup>8</sup> and J Dolinšek<sup>1,2</sup>

<sup>1</sup> J. Stefan Institute and University of Ljubljana, Faculty of Mathematics and Physics, Jamova 39, SI-1000 Ljubljana, Slovenia

<sup>2</sup> EN-FIST Centre of Excellence, Dunajska 156, SI-1000 Ljubljana, Slovenia

<sup>3</sup> NAMASTE Centre of Excellence, Jamova 39, SI-1000 Ljubljana, Slovenia

<sup>4</sup> Institute of Molecular Physics, Polish Academy of Sciences, Smoluchowskiego 17, 60-179 Poznań, Poland

<sup>5</sup> Institute of Mathematics, Physics and Mechanics and University of Ljubljana, Faculty of Civil and Geodetic Engineering, Jamova 2, SI-1000 Ljubljana, Slovenia

<sup>6</sup> Institute of Physics, Laboratory for the Study of Transport Phenomena, Bijenička 46, POB 304, HR-10001 Zagreb, Croatia

<sup>7</sup> Ludwig-Maximilians-Universität München, Department of Earth and Environmental Sciences, Crystallography Section, Theresienstrasse 41, D-80333 München, Germany

<sup>8</sup> Max-Planck-Institut für Chemische Physik fester Stoffe, Nöthnitzer Straße 40, D-01187 Dresden, Germany

E-mail: [jani.dolinsek@ijs.si](mailto:jani.dolinsek@ijs.si)

Received 9 November 2011

Published 7 February 2012

Online at [stacks.iop.org/JPhysCM/24/085703](http://stacks.iop.org/JPhysCM/24/085703)

## Abstract

The PdGa intermetallic compound is a highly selective and stable heterogeneous hydrogenation catalyst for the semi-hydrogenation of acetylene. We have studied single crystals of PdGa grown by the Czochralski technique. The <sup>69</sup>Ga electric-field-gradient (EFG) tensor was determined by means of NMR spectroscopy, giving experimental confirmation of both the recently refined structural model of PdGa and the theoretically predicted Pd–Ga covalent bonding scheme. The hydrogenation experiment has detected no hydrogen uptake in the PdGa, thus preventing *in situ* hydride formation that leads to a reduction of the catalytic selectivity. We have also determined bulk physical properties (the magnetic susceptibility, the electrical resistivity, the thermoelectric power, the Hall coefficient, the thermal conductivity and the specific heat) of single-crystalline PdGa. The results show that PdGa is a diamagnet with metallic electrical resistivity and moderately high thermal conductivity. The thermoelectric power is negative with complicated temperature dependence, whereas the Hall coefficient is positive and temperature-dependent, indicating complexity of the Fermi surface. Partial fulfillment of the NMR Korringa relation reveals that the charge carriers are weakly correlated. Specific heat measurements show that the density of electronic states (DOS) at the Fermi energy of PdGa is reduced to 15% of the DOS of the elemental Pd metal.

(Some figures may appear in colour only in the online journal)

## 1. Introduction

Based on the active-site isolation concept [1], a rational approach to apply intermetallic compounds with ordered

crystal structures as selective, stable and unsupported catalysts in heterogeneous catalysis has been developed recently [2–4]. The basic idea is that isolated active sites on the surface of an intermetallic compound enable only a reduced number of

possible adsorption configurations for the reactants, leading to a narrower range of possible reaction products and improved selectivity. Ordered crystal structures lead to a uniform surrounding of the active sites, so that the number of neighboring sites and the distances between them are well defined. By selecting intermetallic compounds with a suitable crystal structure, the active sites can be tailored to the needs of the reaction. In many intermetallic compounds, strong covalent bonding between the atoms is present (see, e.g., [4, 5]), providing long-term stability of the catalytic material under reaction conditions and avoiding deactivation of the near-surface region *in situ* after a period of time.

The intermetallic compounds from the Pd–Ga system [3, 6, 7], in particular PdGa<sup>9</sup>, and the Al<sub>13</sub>Co<sub>4</sub> complex intermetallic [8] have recently been explored as highly selective heterogeneous hydrogenation catalysts in the semi-hydrogenation of acetylene in a large excess of ethylene, which is an important step in the purification of the ethylene feed for the production of polyethylene. Selectivity is crucial in this reaction, as an unselective catalyst would convert valuable ethylene into ethane and also enable the formation of carbonaceous deposits, which deactivate the catalyst. The selective hydrogenation of acetylene to ethylene on the (100) surface of the Al<sub>13</sub>Co<sub>4</sub> has been investigated theoretically at the atomistic level by *ab initio* density-functional theory (DFT) simulations [8], confirming the usefulness of the active-site isolation concept.

The intermetallic compound PdGa was also proven to follow this concept [2–7, 9, 10]. The crystal structure of PdGa is well ordered. The Pd atoms are surrounded solely by Ga atoms and vice versa [11]. The Ga–Pd interactions were shown by quantum chemical methods to have covalent nature [3, 12], ensuring high stability of the PdGa phase under reaction conditions [6, 7]. A comparison of the catalytic data for the hydrogenation of acetylene to ethylene catalyzed by either the PdGa or the supported Pd/Al<sub>2</sub>O<sub>3</sub> conventional catalyst has shown that PdGa possesses high and stable selectivity, while the supported Pd exhibits low selectivity as well as strong deactivation with time on stream [3].

While the existing experimental studies of the PdGa material were performed on polycrystalline samples, large PdGa single crystals were successfully grown recently by the Czochralski method [13]. Since catalysis proceeds at the surface, well-defined and oriented surfaces prepared from single-crystalline slices are preferred for fundamental studies to those prepared from polycrystalline material. In addition, the underlying bulk is influencing the properties of the surface, so that knowledge of the bulk properties of the material is important to connect catalytic properties of the surface to the structural and electronic properties of the bulk.

In this paper, we present an experimental investigation of the physical properties of single-crystalline PdGa material. By using NMR spectroscopy, we determined the electric-field-gradient (EFG) tensor at the <sup>69</sup>Ga site in the unit

cell and confirm the covalent bonding scheme between the Pd and Ga atoms. We also determined bulk magnetic, electrical and thermal transport properties and specific heat of the PdGa along well-defined crystallographic directions. Hydrogen absorption in the PdGa was studied as well. This work complements the determination of anisotropic bulk physical properties of the complex intermetallic compound Al<sub>13</sub>Co<sub>4</sub> [14], also considered as a selective and stable catalyst in the semi-hydrogenation of acetylene [8].

## 2. Structural considerations and sample preparation

PdGa is a cubic phase crystallizing in the FeSi type of structure, space group *P*2<sub>1</sub>3 (no. 198) with the lattice parameter  $a = 4.8970 \text{ \AA}$  [11]. There are four formula units in the unit cell ( $Z = 4$ ), with four Pd in Wyckoff position 4a,  $xxx$ ,  $x = 0.39240$ , and four Ga in Wyckoff position 4a,  $xxx$ ,  $x = 0.09295$ . The FeSi type of structure may be considered as a strongly distorted NaCl type with an associated increase in coordination number from 6 to 7 for both atom sites [15]. The first coordination shell of Pd or Ga, respectively, consists exclusively of seven atoms of the other kind. This structural arrangement makes the Pd atoms well separated from each other by the surrounding Ga shell, fulfilling the requirement of the active-site isolation for catalytic selectivity. In figure 1(a), the crystal structure of the PdGa is shown, whereas the coordination polyhedron formed by seven Ga atoms around a central Pd atom is shown in figure 1(b) (a similar, but reversed arrangement of seven Pd atoms around the central Ga atom applies also to the first coordination shell of Ga). The shortest contact of  $2.5399 \text{ \AA}$  is between the Pd and Ga atoms located on a threefold symmetry axis (shown by a dashed line in figure 1(b)). The coordination is completed by three slightly longer contacts of  $2.5726 \text{ \AA}$  and three significantly longer contacts at  $2.7058 \text{ \AA}$ . This rare coordination of the atoms is a result of two-center Pd–Ga and three-center Pd–Ga–Pd covalent interactions [3, 12]. The larger distance among Pd atoms ( $3.0084 \text{ \AA}$ ) in comparison to elemental palladium may be the reason for the higher selectivity of PdGa as a hydrogenation catalyst.

Our centimeter-size PdGa-oriented single crystal was grown by the Czochralski method. The details of preparation and material characterization are published elsewhere [13]. For the measurements we have cut from the parent crystal three rectangular bars of dimensions  $7 \times 1 \times 1 \text{ mm}^3$ , with their long axes along the [100], [110] and [111] crystallographic directions, where the perpendicular directions of each bar were known as well. Due to the cubic symmetry of the crystal structure of PdGa, no anisotropy of the bulk physical properties of tensorial character is expected, so that the measurements of some of the investigated quantities (the electrical resistivity and the Hall coefficient) on the three differently oriented samples were performed, mainly to confirm the isotropy of the employed material and hence its structural quality. However, the NMR spectra are sensitive to the site symmetry of the resonant nuclei, which in PdGa is lower than octahedral, so that orientation-dependent studies of the <sup>69</sup>Ga NMR spectra in the magnetic field by rotating the

<sup>9</sup> According to the difference in electronegativity and analysis of chemical bonding [12], the chemical formula of the compound is more correctly written as GaPd instead of PdGa. However, for consistency with the previous literature, we use PdGa in this work.

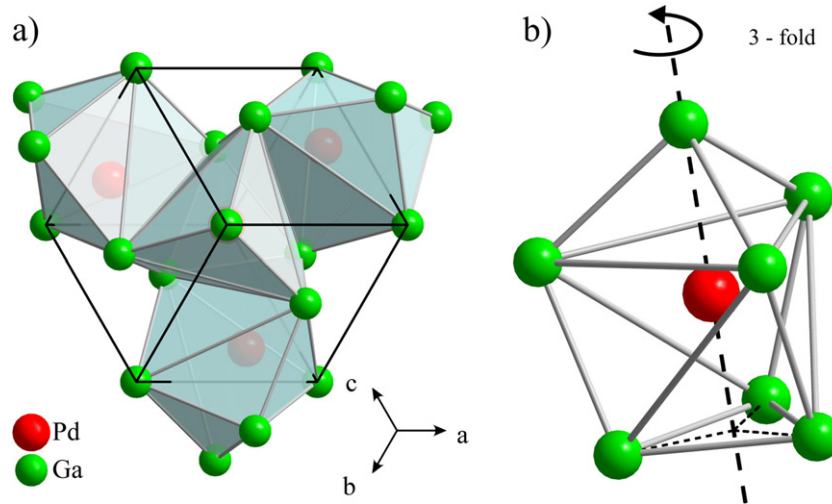


**Figure 1.** (a) The cubic unit cell of PdGa according to [11]. (b) Coordination polyhedron formed by seven Ga atoms around a central Pd atom (the first coordination shell of Pd). A similar, but reversed, arrangement of seven Pd atoms around the central Ga atom also applies to the first coordination shell of Ga. The threefold symmetry axis is shown by a dashed line.

samples around well-defined crystallographic directions are needed to extract the EFG tensor.

### 3. <sup>69</sup>Ga NMR

#### 3.1. <sup>69</sup>Ga EFG tensor and the Knight shift

The <sup>69</sup>Ga nuclei interact with the surrounding ions and electrons by the electrical and magnetic interactions. The <sup>69</sup>Ga nuclear electric quadrupole moment  $Q$  couples to the EFG tensor  $V_{ij}$  of the surrounding ionic and electronic charges via the electric quadrupole interaction, where the charges within the first coordination shell around the Ga atoms give the dominant contribution to the EFG due to  $1/r^3$  radial dependence. The symmetry of the EFG tensor thus reveals the symmetry of the electric charge distribution within the local chemical environment around the resonant nucleus. In the case of Ga–Pd covalent bonding, the largest part of the EFG originates from the valence-electron density. Conduction-electron density contributes to the EFG at the <sup>69</sup>Ga sites as well and the interaction between the conduction electrons and the electrons in the bonding orbitals gives an additional contribution to the electronic EFG via the distortion of the molecular cores. Magnetic coupling between the nucleus and the electrons proceeds via the magnetic shielding tensor  $S_{ij}$  that mediates the interaction between the nuclear spin  $I$  and the external magnetic field  $H_0$ . Magnetic shielding originates from the electronic surrounding and generally contains the chemical shift tensor  $\sigma_{ij}$  due to the electrons in the molecular orbitals and the Knight shift tensor  $K_{ij}$  due to the conduction electrons [16]. The isotropic part of the magnetic shift (the sum of the isotropic chemical shift  $\sigma_{\text{iso}} = (1/3)\text{Tr}\{\sigma_{ij}\}$  and the isotropic Knight shift  $K_{\text{iso}}$  due to the contact interaction between the nuclear spin and the s-type conduction electrons that extend into the nucleus) is usually much larger than the anisotropic part. In addition,  $K_{\text{iso}}$  is typically two orders of magnitude larger than  $\sigma_{\text{iso}}$ , so that it

is a good approximation to describe the magnetic shift by the isotropic Knight shift  $K_{\text{iso}}$  only.

Orientation-dependent <sup>69</sup>Ga NMR spectra were recorded at the temperature of 80 K in a magnetic field of 9.39 T strength, corresponding to the Larmor frequency  $\nu_L$  (<sup>69</sup>Ga) = 96.008 MHz. The crystal was rotated around the crystallographic direction [100], which was enough to extract the <sup>69</sup>Ga EFG tensor from the rotation patterns. According to the PdGa structural model [11], the closest Pd atom to the resonant <sup>69</sup>Ga nucleus (yielding the shortest Pd–Ga bond and consequently the largest EFG-tensor element) is the atom located on the threefold axis (figure 1(b)). By choosing the Z axis of the EFG-tensor principal-axes system (PAS) to point along the threefold direction, the threefold symmetry of the atomic site requires the following form of the <sup>69</sup>Ga EFG tensor in its PAS:

$$V_{ij} = \begin{vmatrix} -V/2 & 0 & 0 \\ 0 & -V/2 & 0 \\ 0 & 0 & V \end{vmatrix}. \quad (1)$$

This form implies that the quadrupole asymmetry parameter is zero,  $\eta = (V_{XX} - V_{YY})/V_{ZZ} = 0$ . Since there are four Ga atoms in the PdGa unit cell, but only one Ga crystallographic site, all four <sup>69</sup>Ga EFG tensors in their PASs are characterized by a single and the same parameter  $V$  (i.e. the four Ga atoms are chemically equivalent). The tensors' PASs are oriented differently with respect to the crystal-fixed coordinate frame, so that one can observe up to four <sup>69</sup>Ga NMR spectral lines in the spectrum at a general orientation of the crystal with respect to the magnetic field direction (i.e. the four Ga atoms are magnetically inequivalent).

Due to the very large electric quadrupole coupling constant  $\nu_Q = e^2qQ/2h$  of the <sup>69</sup>Ga nucleus (spin  $I = 3/2$ ), where  $eq = V$  is the largest EFG-tensor element, we were able to detect only the central transition ( $1/2 \leftrightarrow -1/2$ ) in the NMR spectrum. Figure 2 shows the rotation pattern of the

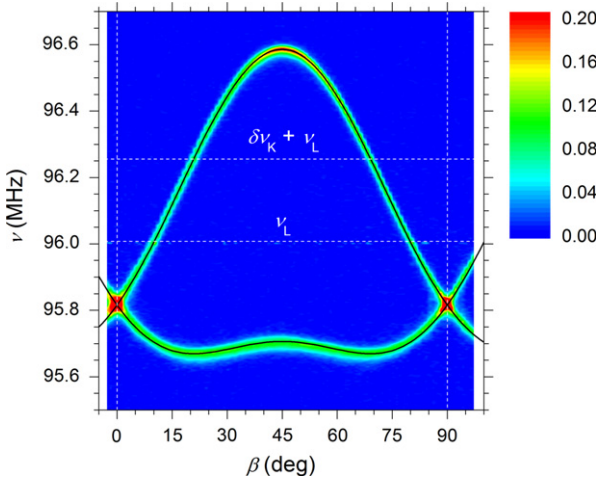


**Figure 2.** Orientation-dependent positions of the  $^{69}\text{Ga}$  NMR spectral lines (the  $1/2 \leftrightarrow -1/2$  central transition) for the rotation of the PdGa monocystal around the  $[100]$  axis. The angle  $\beta = 0$  corresponds to the orientation where one of the cubic axes is parallel to the magnetic field. Black solid curves are fits to equation (3) using a single parameter  $\nu_Q = 13.0$  MHz. The  $^{69}\text{Ga}$  Larmor frequency  $\nu_L$  and the Knight shift (plus the Larmor frequency)  $\delta\nu_K + \nu_L = \nu - \delta\nu_Q$  are shown by horizontal dashed lines.

NMR spectrum around the  $[100]$  direction, where the angle  $\beta = 0$  corresponds to the orientation where one of the cubic axes (say, the  $[010]$  direction) was parallel to the magnetic field. For this rotation we observe two spectral lines, each corresponding to two Ga atoms in the unit cell. The pattern repeats after  $90^\circ$ , as expected for the cubic symmetry of the crystal.

The second-order quadrupole shift of a spin  $I = 3/2$  nucleus is generally written as [17]

$$\delta\nu_Q = -\frac{\nu_Q^2}{2\nu_L} [A(\varphi)\cos^4\theta + B(\varphi)\cos^2\theta + C(\varphi)], \quad (2)$$

where  $\theta$  and  $\varphi$  are Euler angles describing the direction of the magnetic field in the PAS of the EFG tensor. The functions  $A$ ,  $B$  and  $C$  depend on the azimuthal angle  $\varphi$  and the asymmetry parameter  $\eta$ , but reduce to constants for the axially symmetric EFG tensor with  $\eta = 0$ , amounting  $A = -27/8$ ,  $B = 30/8$  and  $C = -3/8$ . By transforming the four  $^{69}\text{Ga}$  EFG tensors of the form given by equation (1) from their respective PASs into the crystal-fixed frame, and allowing the magnetic field to be tilted for an angle  $\beta$  from the cubic axis, we obtain for the  $[100]$  rotation two different second-order quadrupole shifts for the four Ga atoms in the PdGa unit cell (pairs of Ga atoms lead to equivalent shifts):

$$\delta\nu_{Q1,2} = \frac{\nu_Q^2}{2\nu_L} \frac{1}{16} [-8 + 3(1 - \cos 4\beta) \pm 8 \sin 2\beta]. \quad (3)$$

Equation (3) perfectly reproduces the experimental orientation dependence of the two  $^{69}\text{Ga}$  lines (solid curves in figure 2) by a single parameter  $\nu_Q = 13.0$  MHz. To obtain the Knight shift, we subtracted from the measured orientation-dependent peak position frequencies the second-order quadrupolar shift given by equation (3). The resulting Knight shift  $\delta\nu_K = \nu -$

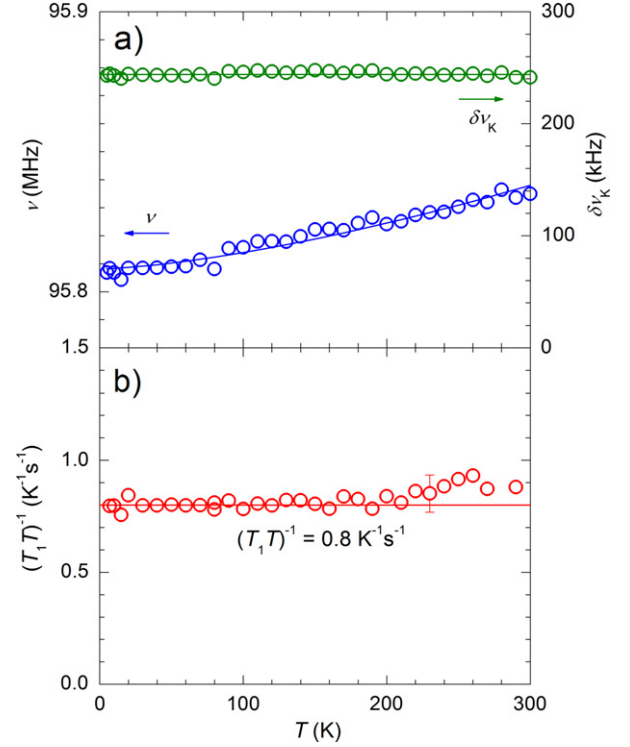


**Figure 3.** (a) Temperature dependence of the  $^{69}\text{Ga}$  NMR line position  $\nu$  for the crystal orientation where one of the cubic axes is parallel to the magnetic field (corresponding to the  $\beta = 0$  orientation in figure 2). The solid curve is the fit to equation (5) and the fitting parameters are described in the text. The temperature independence of the Knight shift  $\delta\nu_K = \nu - \nu_L - \delta\nu_Q(T)$  is demonstrated as well. The horizontal line corresponds to the Knight shift value  $\delta\nu_K = 244$  kHz. (b) Temperature-dependent  $^{69}\text{Ga}$  spin–lattice relaxation rate  $T_1^{-1}$  of PdGa in a  $(T_1 T)^{-1}$  versus temperature plot.

$\nu_L - \delta\nu_Q$  (figure 2) is positive. Its value will be determined in the following by analyzing the temperature dependence of the  $^{69}\text{Ga}$  spectral lines. Here it is important to stress that the entire angular dependence of the  $^{69}\text{Ga}$  lines could be accounted for by the electric quadrupole interaction, so that the assumption of approximating the magnetic shift by the isotropic Knight shift is well justified.

The temperature dependence of the  $^{69}\text{Ga}$  spectral line position was determined for the crystal orientation where one of the cubic axes was parallel to the magnetic field (corresponding to the  $\beta = 0$  orientation in figure 2, where a single line is observed in the spectrum). The temperature-dependent line position in the range between 300 and 4 K is shown in figure 3(a). The line position exhibits slight variation with temperature, which can be reproduced by assuming the quadrupolar coupling constant to obey the following temperature dependence:

$$\nu_Q = \nu_{Q,0}(1 - \alpha T^{3/2}). \quad (4)$$

The  $T^{3/2}$  behavior of  $\nu_Q$  was observed in many metals with the resonant nuclei in a noncubic environment. It was shown [18] that the electronic part of the EFG is responsible for this kind of temperature dependence due to the effect of the electron–phonon interactions on the crystal potential.

The characteristic order of magnitude for the coefficient  $\alpha$  is  $10^{-5} \text{ K}^{-1.5}$ , in particular  $1.5 \times 10^{-5} \text{ K}^{-1.5}$  for Zn and  $2.2 \times 10^{-5} \text{ K}^{-1.5}$  for Cd. Inserting equation (4) into (3) and setting  $\beta = 0$ , the second-order quadrupole shift depends on temperature as

$$\delta\nu_Q = -\frac{\nu_{Q,0}^2}{4\nu_L} (1 - \alpha T^{3/2})^2. \quad (5)$$

This form of  $\delta\nu_Q$  reproduces well the temperature-dependent dataset of figure 3(a) (solid curve) by taking  $\alpha = 6.6 \times 10^{-6} \text{ K}^{-1.5}$ . In addition, from the previously deduced value of  $\nu_Q = 13.0 \text{ MHz}$  at 80 K we obtain the extrapolated zero-temperature value of the quadrupole coupling constant as  $\nu_{Q,0} = 13.06 \text{ MHz}$ . To get the temperature-dependent Knight shift, we subtracted from the data of figure 3(a) the contribution of the second-order quadrupole shift given by equation (5). The remaining Knight shift is temperature-independent (figure 3(a)) and amounts to  $\delta\nu_K = 244 \text{ kHz}$ . The relative Knight shift is then obtained as  $K = \delta\nu_K/\nu_L = 2.54 \times 10^{-3}$ .

### 3.2. $^{69}\text{Ga}$ spin–lattice relaxation and the Korringa relation

NMR spectroscopy offers a criterion on how free-electron-like a metallic compound is. The method relies on the simultaneous measurement of the Knight shift  $K$  and the NMR spin–lattice relaxation rate  $T_1^{-1}$ . For a free-electron gas, a simple equation relating these two quantities, called the Korringa relation [19], holds:

$$K^2 = \frac{\hbar}{4\pi k_B T T_1} \left( \frac{\gamma_e}{\gamma_n} \right)^2, \quad (6)$$

where  $\gamma_e$  and  $\gamma_n$  are the electronic and the nuclear gyromagnetic ratios, respectively. The degree to which this relation is fulfilled, by inserting the experimental values of  $K$  and  $T_1^{-1}$ , is a measure of the free-electron-like nature of the compound.

The temperature-dependent  $^{69}\text{Ga}$  spin–lattice relaxation rate  $T_1^{-1}$  was measured by the inversion-recovery method applied to the central transition. To extract the  $T_1^{-1}$  values, the nuclear magnetization relaxation curves  $M_n(t)$  were analyzed by the model of magnetic relaxation of a spin  $I = 3/2$  nucleus:

$$M_n = M_{n,0} [1 - (1 + s) \{0.1 \exp(-t/T_1) + 0.9 \exp(-6t/T_1)\}], \quad (7)$$

which fitted well the magnetization-recovery curves. Here  $M_{n,0}$  is the thermal-equilibrium nuclear spin magnetization and  $s$  is the portion of the inverted magnetization after the first pulse. The product of the temperature-dependent relaxation rate and the absolute temperature,  $(T_1 T)^{-1}$ , as a function of temperature is shown in figure 3(b). This kind of plot is usually employed for metals, where  $T_1^{-1} \propto T$  due to the coupling of the nuclear spin to the spins of the conduction electrons, so that the product  $T_1 T$  eliminates the temperature dependence. In figure 3(b) we see that the data fall on a constant line  $(T_1 T)^{-1} = 0.8 \text{ K}^{-1} \text{ s}^{-1}$ , confirming the dominant metallic-type relaxation via the

conduction electrons. Inserting the values of  $K$  and  $T_1 T$  into the Korringa relation of equation (6), we obtain the ratio  $K^2 4\pi k_B T_1 T / (\hbar \gamma_e^2 / \gamma_n^2) = 1.75$ , whereas the value 1.0 is expected for the model of independent conduction electrons. This means that the conduction electrons in PdGa are weakly correlated. The obtained value is consistent with the values found for alkali and noble metals, which fall in the range between 1.0 and 2.0 [20].

### 3.3. Discussion of $^{69}\text{Ga}$ NMR results

The experimentally determined axially symmetric form of the  $^{69}\text{Ga}$  EFG tensor in PdGa, which is described by a single parameter  $V$ , is consistent with the threefold symmetric charge distribution around the Ga atoms and therefore supports the structural model [11]. The  $T^{3/2}$  temperature dependence of the quadrupolar shift of the NMR line indicates that the main part of the EFG is of electronic origin (originating from both the conduction electrons and the electrons in the molecular orbitals of the Pd–Ga chemical bonds). The experimental value  $\nu_{Q,0} = 13.06 \text{ MHz}$  allows extraction of the largest principal value of the EFG tensor  $V$  from the equation  $\nu_Q = eQV/2h$  by using the value of the  $^{69}\text{Ga}$  electric quadrupole moment  $Q/|e| = 0.168 \times 10^{-24} \text{ cm}^2$ , yielding  $V = 6.4 \times 10^{21} \text{ V m}^{-2}$ . The  $V$  value of PdGa was also calculated theoretically [12] from first-principles electronic structure calculations performed on the scalar-relativistic DFT level using the full potential APW+lo code WIEN2k [21], by employing the published PdGa structural model. The resulting theoretical value  $V = -5.8 \times 10^{21} \text{ V m}^{-2}$  matches well the experimental one (regarding the sign, recall that NMR cannot determine experimentally the sign of  $V$ , since  $|V|$  is measured). The NMR results thus indirectly confirm the covalent bonding scheme between the Ga and Pd atoms that is required for high stability of the PdGa phase under catalytic conditions.

## 4. Bulk physical properties of PdGa

In order to characterize further the PdGa material, we determined its bulk physical properties by measuring the magnetic susceptibility, the electrical resistivity, the thermoelectric power, the Hall coefficient, the specific heat and the thermal conductivity. Hydrogen absorption from the gas phase was investigated as well. Magnetic measurements were conducted by a Quantum Design MPMS XL-5 SQUID magnetometer equipped with a 50 kOe magnet. The measurements of the electrical resistivity, the thermoelectric power, the Hall coefficient, the thermal conductivity and the specific heat were conducted by a Quantum Design physical property measurement system (PPMS 9T), equipped with a 90 kOe magnet, and home-made equipment. Electrical resistivity was measured by a standard four-terminal technique. The thermoelectric power and the thermal conductivity were measured simultaneously by monitoring both the temperature and voltage drop across the sample after a heat pulse is applied to its end by means of square waves. The Hall coefficient measurements were

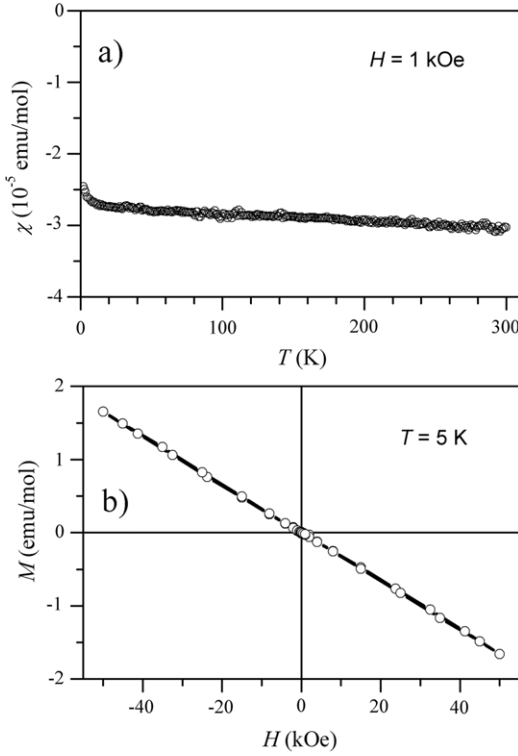


**Figure 4.** (a) Temperature-dependent magnetic susceptibility  $\chi = M/H$  of PdGa in the magnetic field  $H = 1$  kOe. (b) Magnetization versus the magnetic field,  $M(H)$ , at  $T = 5$  K. In both experiments, the magnetic field was applied along the [100] crystallographic direction.

performed by the five-point method using the standard ac technique in magnetic fields up to 10 kOe. The specific heat was measured by a thermal-relaxation calorimeter.

#### 4.1. Magnetic properties

Magnetic susceptibility  $\chi = M/H$  was determined in the temperature range 1.9–300 K in the magnetic field  $H = 1$  kOe applied along the [100] crystallographic direction. The susceptibility (figure 4(a)) is negative diamagnetic and largely temperature-independent, except in the low-temperature limit, where a tiny Curie upturn is observed due to the small amount of paramagnetic impurities (perhaps the residual impurities in the starting materials for the PdGa synthesis). The room-temperature (RT) susceptibility value amounts to  $\chi_{293\text{ K}} = -3 \times 10^{-5}$  emu mol $^{-1}$ . The magnetization versus the magnetic field,  $M(H)$ , experiment performed at  $T = 5$  K for the magnetic sweep  $\pm 50$  kOe is shown in figure 4(b). The negative-sloping  $M(H)$  straight line confirms the diamagnetic nature of PdGa. The Larmor diamagnetic core susceptibility of PdGa was calculated from literature tables [22] to be in the range  $\chi_{\text{dia}} = (-3.3, -2.6) \times 10^{-5}$  emu mol $^{-1}$  for different ionization states of the elements (Pd $^{2+}$ , Pd $^{4+}$  and Ga $^{3+}$ ).  $\chi_{\text{dia}}$  accounts for practically all the susceptibility at RT, so that the two conduction-electron contributions to the susceptibility (the Pauli paramagnetic spin susceptibility and the Landau orbital diamagnetic susceptibility) that are of the same order of magnitude as  $\chi_{\text{dia}}$  largely compensate each other.

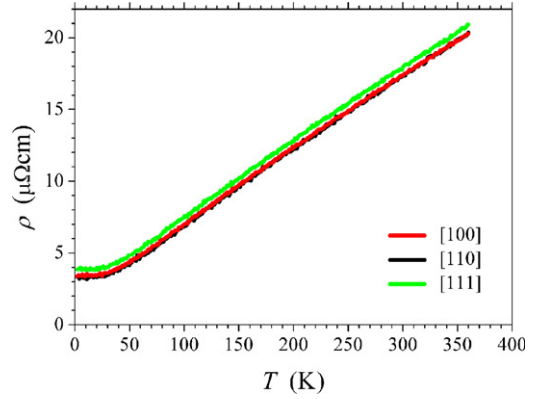


**Figure 5.** Temperature-dependent electrical resistivity  $\rho$  of PdGa for the current along the [100], [110] and [111] crystallographic directions.

#### 4.2. Electrical resistivity

Electrical resistivity  $\rho(T)$  was measured between 360 and 2 K on the three differently oriented PdGa samples by directing the current along [100], [110] and [111] directions, respectively. The results are shown in figure 5. As expected from the cubic symmetry, there is no anisotropy of the resistivity along different crystallographic directions and the small scatter in the absolute values is the experimental error due to uncertainty in the determination of the samples' geometrical parameters (the length and the cross section). Away from the low-temperature limit, the resistivity increases linearly with temperature, where the positive temperature coefficient (PTC) demonstrates the predominant role of the electron–phonon inelastic scattering mechanism in the temperature dependence of  $\rho$ . The saturation of  $\rho$  to a constant plateau in the  $T \rightarrow 0$  limit is due to quenched defects in the structure. The resistivity values are metallic, amounting at RT to  $\rho_{293\text{ K}} = 17.5$   $\mu\Omega\text{cm}$  and the residual resistivity is  $\rho_{2\text{ K}} = 3$   $\mu\Omega\text{cm}$ . For comparison, the RT resistivity of the elemental Pd metal amounts to  $\rho_{293\text{ K}}^{\text{Pd}} = 10.5$   $\mu\Omega\text{cm}$ , so that the RT ratio of the resistivities is  $\rho/\rho^{\text{Pd}} = 1.67$ . PdGa can thus be considered as a good metallic conductor.

#### 4.3. Thermoelectric power

The thermoelectric power is sensitive to the sign of the charge carriers and hence distinguishes between the electrons and the holes. The thermopower (the Seebeck coefficient  $S$ ) of PdGa was measured between 320 and 2 K along the [100] direction and the result is shown in figure 6. The thermopower is small and negative, suggesting the electrons to be the majority charge carriers. Its RT value amounts to  $S_{293\text{ K}} = -3.6$   $\mu\text{V K}^{-1}$ . The detailed temperature dependence of  $S(T)$ , which shows a weakly pronounced local inflection point and a minimum, is difficult to analyze theoretically as this complex behavior may originate from both the complexity of the Fermi surface and the electron–phonon coupling (phonon drag).

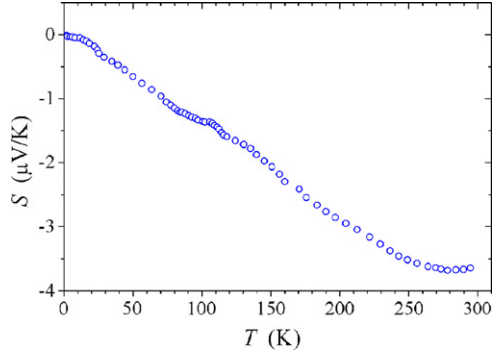


**Figure 6.** Temperature-dependent thermoelectric power  $S$  of PdGa measured along the [100] crystallographic direction.

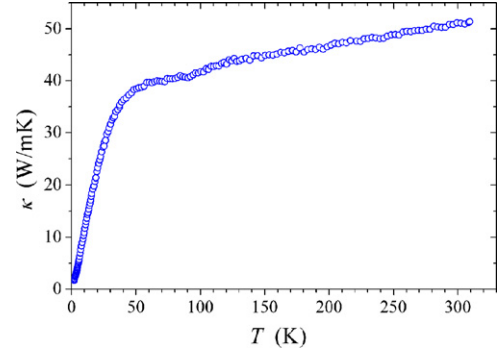


**Figure 8.** Temperature-dependent thermal conductivity  $\kappa$  of PdGa along the [100] crystallographic direction.

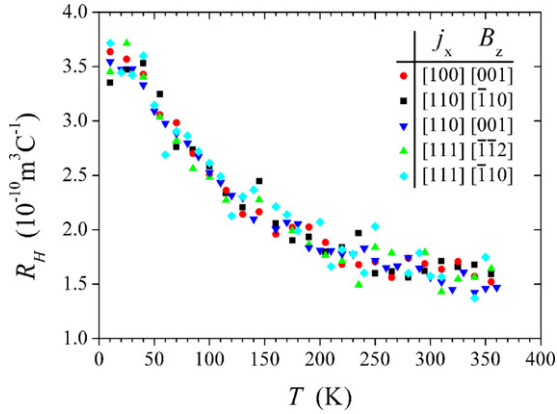


**Figure 7.** Temperature-dependent Hall coefficient  $R_H = E_y/j_x B_z$  of PdGa for five different combinations of the current  $j_x$  and magnetic field  $B_z$  orthogonal directions, given in the legend.

#### 4.4. Hall coefficient

The Hall coefficient is also sensitive to the sign of the charge carriers and distinguishes between the electrons and the holes. The temperature-dependent Hall coefficient  $R_H = E_y/j_x B_z$  was determined between 360 and 10 K. Five sets of experimental data were collected by directing (1) the current  $j_x$  along the [100] direction and the magnetic field  $B_z$  in the [001] direction, (2)  $j_x$  along the [110] direction and  $B_z$  in the perpendicular plane along the [001] and  $[\bar{1}10]$  orthogonal directions, and (3)  $j_x$  along the [111] direction and  $B_z$  in the perpendicular plane along the  $[\bar{1}\bar{1}2]$  and  $[\bar{1}10]$  orthogonal directions. The five  $R_H$  datasets do not show any anisotropy beyond the experimental precision of  $\pm 0.1 \times 10^{-10} \text{ m}^3 \text{ C}^{-1}$  (figure 7). The  $R_H$  values are metallic in the range  $10^{-10} \text{ m}^3 \text{ C}^{-1}$  with the positive RT value of  $R_H^{293 \text{ K}} \approx 1.6 \times 10^{-10} \text{ m}^3 \text{ C}^{-1}$ .  $R_H$  increases upon cooling and remains positive, reaching at 4 K the value  $R_H^{4 \text{ K}} \approx 3.5 \times 10^{-10} \text{ m}^3 \text{ C}^{-1}$ . Due to the metallic  $R_H$  values, this relatively small increase by a factor of about two can be attributed to the temperature-dependent changes of the Fermi surface.

The positive  $R_H$  suggests that the holes are the majority charge carriers, whereas the negative thermopower offers the opposite conclusion that the charge is carried by the electrons. While this apparent contradiction can be resolved

by considering the details of the Fermi surface, opposite-sign  $S < 0$  and  $R_H > 0$  are not uncommon in the literature. This situation was discussed for the high- $T_c$  cuprates [23], where the electrons form an unusual state in which the Hall (cyclotron) mass parallel to the Fermi surface is hole-like ( $< 0$ ) but the transport mass perpendicular to it is electron-like ( $> 0$ ). The electron-like transport mass contributes to negative  $S$ , while the hole-like Hall mass results in positive  $R_H$ . Similar situation was found also in the Y-phase Al–Co–Ni decagonal approximant phase [24].

#### 4.5. Thermal conductivity

The thermal conductivity  $\kappa$  of PdGa along the [100] crystallographic direction is displayed in figure 8.  $\kappa$  increases rapidly in the low-temperature region up to 30 K, whereas at higher temperatures the growth becomes slower. The RT value amounts to  $\kappa_{293 \text{ K}} = 50 \text{ W mK}^{-1}$ , whereas the reference value for the Pd metal is  $\kappa_{298 \text{ K}} = 71.8 \text{ W mK}^{-1}$ . This makes PdGa a moderate thermal conductor.

#### 4.6. Specific heat and the electronic density of states at the Fermi energy $\varepsilon_F$

The low-temperature specific heat  $C(T)$  is a convenient quantity to estimate the value of the electronic density of states (DOS) at the Fermi energy  $\varepsilon_F$  and the Debye temperature  $\theta_D$ . For the diamagnetic PdGa, the total specific heat is a sum of the electronic and lattice specific heats. The electronic specific heat depends linearly on temperature,  $C_{\text{el}}(T) = \gamma T$ , with the electronic specific heat coefficient  $\gamma = (\pi^2/3)k_B^2 g(\varepsilon_F)$ , where  $g(\varepsilon_F)$  is the DOS at  $\varepsilon_F$ . At low temperatures below about 10 K, the lattice specific heat can usually be well approximated by the Debye model and is expressed as a function of temperature in the form  $C_{\text{lat}}(T) = \alpha T^3$ . The lattice specific heat coefficient  $\alpha$  is related to the Debye temperature via the relation  $\theta_D = (12\pi^4 R/5\alpha)^{1/3}$ , where  $R$  is the gas constant. The total specific heat at low temperatures can then be written as

$$C(T) = \gamma T + \alpha T^3. \quad (8)$$

The specific heat measurements were performed in the temperature range between 2 and 300 K. The low-temperature

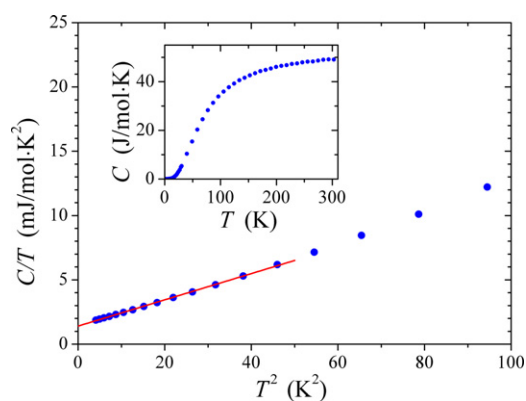


**Figure 9.** Low-temperature molar specific heat of PdGa in a  $C/T$  versus  $T^2$  plot. The solid line is the fit with equation (8). The specific heat in the entire investigated temperature range (2–300 K) is displayed in the inset.

molar specific heat is displayed in figure 9 in a  $C/T$  versus  $T^2$  plot, whereas the specific heat in the entire investigated temperature range is displayed in the inset. The analysis yielded the values  $\gamma = 1.41 \text{ mJ mol}^{-1} \text{ K}^{-2}$  and  $\theta_D = 267 \text{ K}$ . The reference values for the elemental Pd metal are [25]  $\gamma_{\text{Pd}} = 9.36 \text{ mJ mol}^{-1} \text{ K}^{-2}$  and  $\theta_D^{\text{Pd}} = 272 \text{ K}$ . The gamma values allow estimating the value of the DOS  $g(\varepsilon_F)$  of PdGa relative to the Pd metal. We obtain  $\gamma/\gamma_{\text{Pd}} = g/g_{\text{Pd}} = 0.15$ , so that the DOS at  $\varepsilon_F$  of PdGa is reduced to 15% of the DOS of the Pd metal. The reduced DOS at  $\varepsilon_F$  is one of the reasons for the higher electrical resistivity of PdGa, as compared to the Pd metal.

#### 4.7. Hydrogen absorption

A good hydrogenation catalyst should show no hydrogen uptake, as the hydride formation involves changes of the structural and electronic properties of the material that directly influence its catalytic performance, resulting in reduced catalytic selectivity and mechanical instability. In order to check for the hydrogen uptake from the gas phase, bulk pieces of PdGa single-crystalline material were placed in a 316 stainless-steel Sievert apparatus under 55 bar of hydrogen gas at 350 °C for 16 h. After reducing the temperature to RT, the sample spent an additional three days in 50 bar hydrogen atmosphere. Hydrogen uptake was measured thermogravimetrically and by the mass spectrometer by detecting desorbed hydrogen in a heating run. While thermogravimetry (TG) detects mass changes of the hydride material, mass spectrometry provides valuable information about the distribution of hydrogen desorption temperatures, which are related to the hydrogen bonding energies in the host metallic material. The PdGa sample was subjected to controlled temperature program of a TG-DTA/DSC Gas Analytical System QMS 403 C Aëolos thermal analyzer with an attached mass spectrometer, capable of detecting minute quantities of hydrogen down to 0.005 mass%. The sample was placed in an alumina pot and attached to a thermocouple on the microbalance. After three evacuation/argon refill cycles, the sample was heated from RT to 800 °C with a

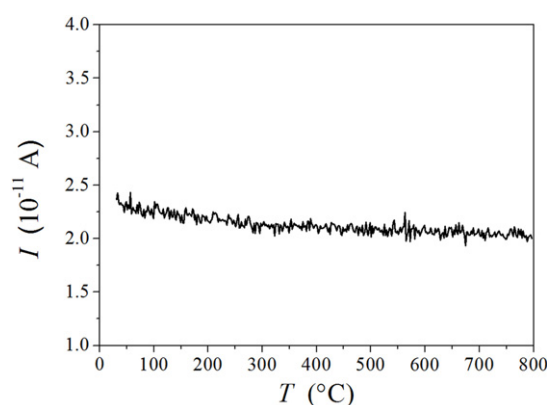


**Figure 10.**  $\text{H}_2$  mass spectrum of PdGa upon heating the material from RT up to 800 °C. The sample was previously subjected to 55 bar of hydrogen gas at 350 °C for 16 h and then left for an additional three days in 50 bar at RT. The vertical axis displays the current of ionized  $\text{H}_2$  molecules. The current value  $I \approx 2 \times 10^{-11} \text{ A}$  corresponds to the background current. No hydrogen release can be noticed during heating, indicating no hydrogen uptake under the above conditions.

20 °C  $\text{min}^{-1}$  heating rate. The upper temperature of the heating run was selected by considering that any stable metal hydride will decompose until 600 °C, so that heating up to 800 °C should be enough to release all the eventually absorbed hydrogen. The mass change of the sample and the hydrogen molecule counts by the mass spectrometer were measured simultaneously. The mass change was found below the detection limit of our measurement system (where the background variations are about 0.005 mass%). No hydrogen release could be noticed also in the  $\text{H}_2$  mass spectrum up to the highest temperature (figure 10). The vertical axis of the spectrum shown in figure 10 displays the current of ionized  $\text{H}_2$  molecules and the measured current value  $I \approx 2 \times 10^{-11} \text{ A}$  corresponds to the background current, in the absence of any hydrogen release. This demonstrates that PdGa does not absorb hydrogen, as required for a good hydrogenation catalyst material.

## 5. Summary and conclusions

Our determination of the  $^{69}\text{Ga}$  EFG tensor by means of NMR spectroscopy gives experimental confirmation of both the recently refined structural model of PdGa [11] and the theoretically predicted Pd–Ga covalent bonding scheme of this hydrogenation catalyst intermetallic compound [3]. Due to structural reasons, PdGa fulfills the criterion of the site-isolation concept needed for high selectivity in a catalytic reaction, whereas strong covalent bonding provides long-term chemical stability of the catalytic material under the reaction condition. Together with the absence of hydrogen absorption, this prevents reduction of the catalytic selectivity of the near-surface region *in situ* after a period of time.

Since heterogeneous catalysis proceeds at the surface, well-defined and oriented surfaces prepared from single-crystalline slices are preferred for fundamental studies to those prepared from polycrystalline material. In addition, the

underlying bulk is influencing the properties of the surface, so that knowledge of the bulk properties of the material is important to connect catalytic properties of the surface to the structural and electronic properties of the bulk. For that purpose we have determined bulk physical properties of the single-crystal PdGa grown by the Czochralski method, by performing measurements along well-defined crystallographic directions. Magnetic measurements have shown that the PdGa material is diamagnetic. The negative thermoelectric power and the positive Hall coefficient suggest a complex Fermi surface. PdGa is a good electrical conductor and a moderate thermal conductor. Partial fulfillment of the NMR Korringa relation reveals that the charge carriers are, to some extent, correlated. Specific heat measurements have shown that the DOS of PdGa at the Fermi energy is reduced to 15% of the DOS of the elemental Pd metal. We believe that our data on the bulk physical properties of PdGa may serve in future atomistic-level studies of the catalytic processes on well-oriented surfaces of this interesting hydrogenation catalyst material.

## Acknowledgments

This work was carried out within the activities of the COST Action CM0904 'Network for Intermetallic Compounds as Catalysts for Steam Reforming of Methanol'. AS, PP and JI acknowledge support by the Croatian Ministry of Science, Education and Sports, grant 035-0352826-2848.

## References

- [1] Sachtler W M H 1976 *Catal. Rev. Sci. Eng.* **14** 193
- [2] Armbrüster M, Kovnir K, Behrens M, Teschner D, Grin Yu and Schlögl R 2010 *J. Am. Chem. Soc.* **132** 14745
- [3] Kovnir K, Armbrüster M, Teschner D, Venkov T V, Jentoft F C, Knop-Gericke A, Grin Yu and Schlögl R 2007 *Sci. Technol. Adv. Mater.* **8** 420
- [4] Armbrüster M, Kovnir K, Grin Yu and Schlögl R 2011 *Complex Metallic Alloys: Fundamentals and Applications* ed J M Dubois and E Belin-Ferré (Weinheim: Wiley-VCH) pp 385–99
- [5] Armbrüster M, Schnelle W, Cardoso-Gil R and Grin Yu 2010 *Chem. Eur. J.* **16** 10357
- [6] Osswald J, Giedigkeit R, Jentoft R E, Armbrüster M, Girgsdies F, Kovnir K, Grin Yu, Schlögl R and Ressler T 2008 *J. Catal.* **258** 210
- [7] Osswald J, Kovnir K, Armbrüster M, Giedigkeit R, Jentoft R E, Wild U, Grin Yu, Schlögl R and Ressler T 2008 *J. Catal.* **258** 219
- [8] Krajčič M and Hafner J 2011 *J. Catal.* **278** 200
- [9] Kovnir K, Teschner D, Armbrüster M, Schnörch P, Hävecher M, Knop-Gericke A, Grin Yu and Schlögl R 2008 *BESSY Highlights 2007* (Berlin: BESSY) p 22
- [10] Kovnir K, Osswald J, Armbrüster M, Giedigkeit R, Ressler T, Grin Yu and Schlögl R 2006 *Stud. Surf. Sci. Catal.* **162** 481
- [11] Armbrüster M, Borrmann H, Wedel M, Prots Yu, Giedigkeit R and Gille P 2010 *Z. Kristallogr. NCS* **225** 617
- [12] Armbrüster M, Giedigkeit R, Ormeci A, Schnelle W, Wagner F R and Grin Yu 2010, unpublished
- [13] Gille P, Ziemer T, Schmidt M, Kovnir K, Burkhardt U and Armbrüster M 2010 *Intermetallics* **18** 1663
- [14] Dolinšek J, Komelj M, Jeglič P, Vrtnik S, Stanić D, Popčević P, Ivkov J, Smontara A, Jagličić Z, Gille P and Grin Yu 2009 *Phys. Rev. B* **79** 184201
- [15] Pauling L and Soldate A M 1948 *Acta Crystallogr.* **1** 212
- [16] See, e.g., Mehring M 1976 *High Resolution NMR Spectroscopy in Solids, NMR—Basic Principles and Progress* vol 11, ed P Diehl, E Fluck and R Kosfeld (Berlin: Springer) p 7
- [17] Freude D, Haase J, Klinowski J, Carpenter T A and Ronikier G 1985 *Chem. Phys. Lett.* **119** 365
- [18] Jena P 1976 *Phys. Rev. Lett.* **36** 418
- [19] Winter J 1971 *Magnetic Resonance in Metals* (Oxford: Clarendon) pp 34–42
- [20] Walstedt R E 2008 *The NMR Probe of High-Tc Materials (Springer Tracts in Modern Physics)* (Berlin: Springer) p 36
- [21] Blaha P, Schwarz K, Madsen G K H, Kvasnicka D and Luitz J 2001 *Computer Code WIEN2k, An Augmented Plane Wave + Local Orbitals Program for Calculating Crystal Properties* ed K Schwarz (Vienna: Technische Universität Wien)
- [22] Selwood P W 1956 *Magnetochemistry* (New York: Interscience) p 78
- [23] Kubo Y 1994 *Phys. Rev. B* **50** 3181
- [24] Smontara A *et al* 2008 *Phys. Rev. B* **78** 104204
- [25] Hsiang T Y, Reister J W, Weinstock H, Crabtree G W and Vuillemin J J 1981 *Phys. Rev. Lett.* **47** 523